Published in final edited form as:
Traffic. 2009 August ; 10(8): 1143–1156. doi:10.1111/j.1600-0854.2009.00935.x.

The Calcium Channel Mucolipin-3 is a Novel Regulator of Trafficking Along the Endosomal Pathway

Jose A. Martina, **Benjamin Lelouvier**, and **Rosa Puertollano**
Laboratory of Cell Biology, National Heart, Lung, and Blood Institute, National Institutes of Health, Bethesda, Maryland 20892, USA

Abstract

The varitint-waddler phenotype in mice is caused by gain-of-function mutations in mucolipin-3 (MCOLN3), a member of the mucolipin family of ion channels. These mice are characterized by defects in pigmentation, hearing loss and vestibular defects, suggesting that MCOLN3 might play a role in melanosome trafficking and hair cell maturation. Recent evidence has shown that MCOLN3 is a Ca2+–permeable channel and its activity is regulated by pH. Here we show that MCOLN3 primarily localizes to early and late endosomes in human epithelial cells. This distribution at the less acidic portions of the endocytic pathway is consistent with the reported inactivation of the channel by low pH. Furthermore, overexpression of MCOLN3 causes dramatic alterations in the endosomal pathway, including enlargement of Hrs-positive endosomes, delayed degradation of epidermal growth factor (EGF) and EGF receptor (EGFR) and defective autophagosome maturation, whereas depletion of endogenous MCOLN3 enhances EGFR degradation. Finally, we found that endosomal pH is higher in cells overexpressing MCOLN3 and propose a model in which Ca2+ release from endosomes mediated by MCOLN3 might be important for efficient endosomal acidification. Therefore, MCOLN3 is a novel Ca2+ channel that plays a crucial role in the regulation of cargo trafficking along the endosomal pathway.

Keywords

autophagy; EGFR; endosomes; mucolipin; TRP

Mucolipins are a family of ion channels that belongs to the superfamily of transient receptor potential (TRP) channels. In mammals, the mucolipin family comprises three members, mucolipin-1, -2 and -3 (MCOLN1–3), that exhibit a common six-membrane-spanning topology. MCOLN1 is the best-characterized member of the family due to the fact that mutations in this protein are associated with a human disease known as mucolipidosis type IV (MLIV). MLIV is a lysosomal storage disorder characterized by acute neurological and ophthalmologic defects (1–3). Heterologous expression of MCOLN1 in several cell types showed that the protein mainly localizes to late endosomes and lysosomes (4–6), and the two di-leucine sorting motifs that regulate trafficking of MCOLN1 have been identified (4–8).

The conductance properties of MCOLN1 remain controversial, as different studies have reported specificity of the channel for Ca2+(9,10), H+(11) and Fe2+(12). In addition, MCOLN1 channel activity can be modulated by phosphorylation (13) and by changes in pH and Ca2+ concentration (10,14,15).

*Correspondence: Rosa Puertollano, puertolr@mail.nih.gov.

The accumulation of enlarged vacuoles that contain different types of undigested lipids is a hallmark of MLIV cells and has lead to the suggestion that MCOLN1 might regulate membrane trafficking at the late endocytic pathway (16,17). However, additional roles have been proposed for MCOLN1 in lysosomal acidification (15,18), autophagosome degradation (19), lysosomal secretion (20) and iron homeostasis (12).

The channel properties and function of MCOLN2 are much less characterized. The protein is expressed in B-lymphocytes and its expression is regulated by the Bruton's tyrosine kinase, a crucial protein in B-lymphocyte development, suggesting that MCOLN2 might play a role in the regulation of immune response (21,22). Recently it has been reported that MCOLN2 localizes to the Arf6-regulated pathway in HeLa cells. Expression of a dominant-negative version of MCOLN2 considerably reduces the amount of internalized CD59 that travels back to the cell surface, suggesting that MCOLN2 could regulate the recycling of certain glycosylphosphatidylinositol-anchored proteins to the plasma membrane (23).

MCOLN3 is a 553-amino acid protein with a predicted mass of 64 kDa, and shows about 75% amino acid similarity with MCOLN1 and MCOLN2. The predicted topology of MCOLN3 consists of six transmembrane-spanning domains with the amino- and carboxy-terminal tails oriented within the cytosol. The region of greatest homology with the other members of the TRP family lies in transmembrane segments 3–6 (amino acids 336–492), which includes the pore formed by segments 5 and 6 (amino acids 448–462). Mutations in MCOLN3 are the cause of the varitint-waddler phenotype in mice, characterized by hearing loss, vestibular dysfunction (circling behavior, head-bobbing, waddling) and coat color dilution (24–27). The mutation in MCOLN3 responsible for this phenotype is an alanine-to-proline mis-sense mutation within the fifth transmembrane domain (A419P). A second mutation, consisting on the substitution of an isoleucine for a threonine residue in the second extracellular loop (I362T), seems to have arisen in the original varitint-waddler stock and attenuates the phenotypic effects of the A419P mutation (28,29). Thus, mice homozygous for the A419P mutation exhibit the most severe phenotype (complete absence of coat pigmentation, high embryonic lethality and sterility), while mice heterozygous for A419P and homozygous for I362T present an intermediate phenotype, and I362T heterozygotes show a very mild phenotype (partial hearing, small defects on pigmentation and no vestibular defects).

Whole cell patch clamp experiments revealed that MCOLN3 is an inwardly (from lumen into cytoplasm) rectifying monovalent cation channel permeable to Ca^{2+}. The channel activity of MCOLN3 is regulated by luminal pH; specifically the channel is suppressed at high H^+ concentration (pH 6.0 and lower) (30,31). A group of three histidine residues (H252, H273, H283) located in the first extracellular loop of the protein seems to be responsible for the H^+–dependent inhibition of the channel (32). Interestingly, the A419P mutation dramatically increases the channel activity of MCOLN3. It has been suggested that the inclusion of a proline residue in the fifth transmembrane domain may induce a conformational change that promotes opening of the pore (29,30,33). Alternatively, the A419P mutation may disrupt channel regulation eliminating the pH-dependent inhibition of the channel (32). In any case, it is important to note that the varitint-waddler phenotype is the consequence of a gain-of-function mutation of MCOLN3. Constitutively active MCOLN3 may mediate massive entry of Ca^{2+} into the cells leading to apoptosis and cell death. In agreement with this idea, heterologous expression of MCOLN3-A419P in melanocytes induces cell death and it has been proposed that death of melanocytes in the inner ear and the skin (two tissues in which the expression of MCOLN3 is high) might be responsible for the hearing problems and the coat color dilution observed in varitint-waddler mice (34).

Nevertheless, the cellular function of wild-type MCOLN3 remains undetermined. In mice, endogenous MCOLN3 has been located to unidentified vesicles in the cytoplasm of hair cells as well as the plasma membrane of the stereocilia (26). In this study we performed a careful characterization of the intracellular distribution of MCOLN3 in the retinal epithelial cell line ARPE19. We found that MCOLN3 is mainly localized to early and late endosomes. Overexpression of MCOLN3 caused enlargement of endosomal structures that were positive for Hrs (hepatocyte growth factor-regulated tyrosine kinase substrate). Moreover, in cells overexpressing MCOLN3 the trafficking of epidermal growth factor (EGF) was altered and there was a considerable delay in the degradation of EGFR (epidermal growth factor receptor). Finally, overexpression of MCOLN3 also caused accumulation of LC3-positive vacuoles and decreased degradation of autophagosomes. Altogether, our data indicate that MCOLN3 regulates trafficking of proteins along the endosomal pathway.

Results

MCOLN3 localizes to the endosomal pathway in human epithelial cells

We addressed the distribution of MCOLN3 in the human retinal pigmented epithelial cell line ARPE19 (35), which has been extensively used as a model system in multiple studies (36,37). ARPE19 cells are polarized, possessing a highly specialized endosomal system, and express endogenous MCOLN3 as revealed by quantitative Reverse Transcription-Polymerase Chain Reaction (Q-RT-PCR) analysis (Figure 7).

The complete open reading frame of MCOLN3 was isolated from a human kidney complementary DNA (cDNA) library and cloned into the pMonomeric-GFP-C1 vector to produce a chimera that expresses green fluorescent protein (GFP) at the N-terminus of MCOLN3 (GFP-MCOLN3). We established that the addition of the GFP tag did not affect the channel activity or specificity of MCOLN3 (data not shown). Transient expression of GFP-MCOLN3 in ARPE19 cells revealed that the protein mainly localizes to the plasma membrane and intracellular vesicles (Figure 1A).

To determine the subcellular localization of GFP-MCOLN3 in more detail, cells were immunostained with antibodies against specific compartments of the endosomal pathway (Figure 1A and B). We found that 60% of the GFP-MCOLN3 positive vesicles also contained Hrs (59.84% SD ± 7.3, n = 707). Colocalization with other early endosomal markers such as EEA1 (10.6% SD ± 1.5, n = 365) and sorting nexin-2 (SNX2) (7.98% SD ± 3.14, n = 653) was much lower (Figure 1B). These data indicate that GFP-MCOLN3 localizes to a subfraction of early endosomes that are starting to mature into late endosomes.

We also found a high incidence of colocalization of GFP-MCOLN3 with late endosomal/lysosomal markers such as lysobiphosphatidic acid (LBPA) (52.91% SD ± 12.21, n = 1203), CD63 (61.43% SD ± 9.6, n = 623) and Lamp-1 (50.34% SD ± 9.5, n = 1913) (Figure 1A and B). In contrast, no colocalization was found with the Golgi marker GM130 (data not shown).

To corroborate these data we also made a functional fusion of the red fluorescent protein mCherry to the amino-terminus of MCOLN3 (Cherry-MCOLN3). We found that Cherry-MCOLN3 extensively colocalizes with GFP-Hrs in vesicular structures (Figure 1C). These data show that GFP-MCOLN3 is mainly located to early and late endosomes, although we cannot rule out that a fraction of the protein is present in lysosomes.

It was previously described that transiently expressed MCOLN3 remains trapped in the endoplasmic reticulum (ER) unless coexpressed with MCOLN1 or MCOLN2 (5); however, we did not observe retention of MCOLN3 in the ER in ARPE19 cells. To solve this discrepancy, we compared the distribution of transiently expressed MCOLN3 between

control and MLIV fibroblasts. As seen in Figure S1, MCOLN3 localized to plasma membrane and intracellular vesicles (many of which were positive for CD63) in both cell types, indicating that MCOLN1 is not necessary for transport of MCOLN3 to the endosomal system. Although we cannot discard the possibility that endogenous MCOLN2 is sufficient to promote exit of MCOLN3 from the ER in MLIV cells, this seems improbable as the levels of recombinant MCOLN3 were over 10 000-fold higher than the levels of endogenous MCOLN2 as measured by quantitative RT-PCR (data not shown).

Overexpression of MCOLN3 causes enlargement of Hrs-positive endosomes

Next we sought to determine the effect of MCOLN3 overexpression on the endosomal pathway. In order to achieve high levels of protein expression, we generated recombinant adenoviruses expressing either GFP-MCOLN3 (Ad. GFP-MCOLN3) or GFP alone (Ad. GFP). As seen in Figure 2, infection of ARPE19 cells with the adenovirus expressing GFP did not cause measurable changes in the distribution or morphology of Hrs-positive vesicles, which showed a similar pattern to the one found in uninfected cells. In contrast, infection with Ad. GFP-MCOLN3 caused a dramatic enlargement of Hrs-labeled structures that seemed to accumulate close to the perinuclear region of the cell (Figure 2). Both Hrs and GFP-MCOLN3 clearly colocalize to the same enlarged early endosomes induced by MCOLN3 overexpression (see inset in Figure 2). Therefore, we observed remarkable alterations in the morphology of the endosomal pathway in cells overexpressing GFP-MCOLN3.

Overexpression of MCOLN3 affects EGFR trafficking

To analyze whether the accumulation of Hrs-positive endosomes induced upon GFP-MCOLN3 overexpression correlates with defects in trafficking of proteins along the endosomal pathway, we monitored delivery of EGF and EGFR from the plasma membrane to lysosomes. EGFR is a prototypical member of the receptor tyrosine kinase family and its activation and trafficking have been extensively characterized. Ligand binding results in dimerization (38), activation and autophosphorylation of the receptor followed by the subsequent binding and phosphorylation of downstream signaling proteins (39). Termination of EGFR signaling occurs via endocytosis and delivery of the receptor to lysosomes for degradation.

We first examined the fate of the internalized EGF over time. ARPE19 cells were infected with adenovirus expressing GFP or GFP-MCOLN3. Forty hours after infection, cells were incubated with Alexa-EGF for 10 min and chased for 1, 2 or 3 h. In control cells the disappearance of internalized EGF was essentially complete after 3 h (Figure 3A). In cells overexpressing GFP-MCOLN3, however, a substantial amount of internalized EGF could still be detected at this time (Figure 3A). EGF remained trapped in enlarged GFP-MCOLN3-positive structures at 3 h after internalization (Figure 3B). Furthermore, ≅70% (67.7% SD ± 5.5, n = 836) of the vesicles positive for EGF and MCOLN3 also contained Hrs, suggesting that they correspond to early endosomes (Figure S2). These experiments indicate that increased levels of MCOLN3 impair EGF degradation and cause accumulation of internalized EGF into aberrant early endosomes.

To corroborate our data we also monitored degradation of EGFR after ligand stimulation. We stimulated cells with EGF for different periods of time and determined the amount of remaining EGFR by immunoblot analysis. Interestingly, we observed that EGFR degradation was considerably delayed in GFP-MCOLN3 expressing cells when compared to cells expressing GFP alone (Figure 4A). Quantitative analysis of three independent experiments revealed that GFP-MCOLN3 overexpression resulted in a 40% increase in the fraction of EGFR that remained undegraded after 4 h of EGF induction compared with

control cells (Figure 4B). Therefore, our results suggest that MCOLN3 has a role in sorting and/or degradation of activated EGF receptors.

Cells overexpressing MCOLN3 also showed evident accumulation of ubiquitin at enlarged Hrs-positive endosomes (Figure 5). These data indicate that MCOLN3 overexpression not only delays EGFR degradation but may also have a broader effect in the trafficking of ubiquitinated proteins along the endosomal pathway.

Increased levels of MCOLN3 do not affect EGFR internalization

To determine whether the effect of overexpressing GFP-MCOLN3 on the downregulation of EGFR was due to a change in the internalization of EGFR, ARPE19 cells overexpressing GFP-MCOLN3 or GFP alone were tested for their ability to internalize Alexa-EGF. We did not find any noticeable difference in the amount of internalized Alexa-EGF in cells overexpressing GFP-MCOLN3 or GFP as measured by confocal immunofluorescence microscopy (Figure 3A), indicating that overexpression of MCOLN3 has little effect on ligand-induced endocytosis of EGFR.

To confirm these data, we also monitored EGFR internalization by using 125I-labeled EGF as ligand (Figure 6). Mock- and adenovirus-infected cells expressing GFP-MCOLN3 were serum-starved, and stimulated with 125-IEGF for different periods of time. Endocytosis of EGFR was very fast in ARP19 cells and by 5 min over 50% of the label was intracellular. Quantitative analysis of three independent experiments revealed no statistically significant differences in the amount of 125I-EGF internalized after ligand stimulation in MCOLN3 expressing cells compared with control cells (Figure 6). Taken together, our data suggest that MCOLN3 inhibits downregulation of EGFR by affecting delivery of the receptor to lysosomes for degradation.

Depletion of endogenous MCOLN3 accelerates EGFR degradation

The decreased EGFR degradation caused by overexpression of MCOLN3 prompted us to investigate whether depletion of endogenous MCOLN3 might also have an effect on the delivery of EGFR to lysosomes. To deplete endogenous MCOLN3, we transfected ARPE19 cells with specific siRNAs. Because antibodies that recognize endogenous MCOLN3 are not commercially available, the efficiency of MCOLN3 siRNA was assessed by Q-RT-PCR. As seen in Figure 7A, we achieved close to 90% reduction in the levels of MCOLN3 messenger RNA (mRNA) after 72 h transfection with MCOLN3 siRNA when compared with cells transfected with control nontarget siRNA.

The kinetics of EGFR degradation was examined at 72 h after transfection with nontarget or MCOLN3 siRNAs. Interestingly, we observed that the rate of EGFR degradation was enhanced at all time points after ligand stimulation in cells treated with MCOLN3 siRNA compared with cells treated with control siRNA (Figure 7B). Quantitative analyses of three independent experiments revealed over 40% reduction in the amount of remaining EGFR at 90 and 120 min after ligand stimulation in MCOLN3-depleted cells when compared with control cells (Figure 7C). Our results confirm a role of MCOLN3 in the trafficking of EGFR to lysosomes.

Abnormalities at the endosomal pathway induced by overexpression of MCOLN3 cause defective autophagic degradation

Recent evidence has shown that defects in the endosomal pathway affect autophagic degradation (19,40–42). Autophagy is a crucial clearance mechanism that prevents accumulation of protein aggregates and abnormal organelles (43–45). The last step of autophagy requires fusion of autophagosomes with the endosomal system to guarantee the

degradation of the autophagosome's content. Autophagosomes can fuse with lysosomes to produce autolysosomes, but they also undergo fusion with earlier parts of the endocytic pathway (46–49). The pre-autolysosomal compartments containing both autophagic and endocytic material are known as amphisomes (50).

To determine whether the alterations of the endosomal pathway caused by MCOLN3 overexpression also affected autophagic degradation, we analyzed the distribution of LC3 in cells transiently expressing GFP-MCOLN3. LC3 is considered to be one of the most specific markers for autophagosomes. Under normal conditions the majority of LC3 is cytosolic; however, after autophagy induction LC3 is lipidated and recruited to the autophagosome's membrane. As expected, LC3 was mostly cytosolic in nontransfected ARPE19 cells, although occasional small LC3-labeled vesicles could be observed (Figure 8A). In contrast, cells expressing GFP-MCOLN3 showed a dramatic accumulation of LC3-positive structures (see arrow in Figure 8A). Colocalization experiments determined that over 75% (76.47% SD ± 10.3, n = 764) of the LC3-positive vesicles also contained GFP-MCOLN3 while 55% (54.62% SD ± 10.36, n = 557) were positive for LC3, GFP-MCOLN3 and CD63 suggesting that they correspond to amphisomes (Figure 8B). In addition, 15% (14.9% SD ± 9.3, n = 164) of the LC3-positive vesicles contained CD63 but not GFP-MCOLN3; these likely correspond to autolysosomes (Figure 8B). Therefore, the majority of LC3 accumulates at the endosomal pathway suggesting that fusion of autophagosomes with endosomes/lysosomes is not blocked by MCOLN3 overexpression but degradation is impaired.

Autophagy can also be monitored by immunoblot, as the lipidated form of LC3 (also known as LC3II) migrates faster than the nonlipidated LC3 (LC3I) during SDS-PAGE. We prepared lysates from mock-infected cells and from cells infected with adenovirus expressing GFP or GFP-MCOLN3. As seen in Figure 8C, a robust increase in the level of LC3II was observed in cells expressing GFP-MCOLN3, confirming that MCOLN3 causes alterations in the autophagic process. Quantification of four independent experiments showed a 20-fold increase in the LC3II/LC3I ratio in MCOLN3-overexpressing cells (Figure 8D). We observed considerable variation in the LC3II/LC3I ratio among different experiments (varying from a minimum of 11-fold increase to a maximum of 38-fold increase). This is probably due to variability in the level of MCOLN3 overexpression; however, it was clear that MCOLN3 caused a dramatic increase in the levels of LC3II. We also observed a significant accumulation of LC3-positive vesicles in cells infected with Ad. GFP-MCOLN3 when compared with cells infected with Ad. GFP as revealed by confocal microscopy (data not shown).

To confirm that increased levels of LC3II after MCOLN3 overexpression were due to impaired autophagosome degradation, we starved cells expressing Ad. GFP or Ad. GFP-MCOLN3 to further induce accumulation of autophagosomes, then allowed cells to recover for 20 min in nutrient-rich medium to permit autophagosome degradation. Quantification of the total number of autophagosomes per cell revealed that after the 20-min recovery period only 22% (n = 93) of the cells expressing GFP showed more than 20 autophagosomes. In contrast, 59% (n = 71) of the cells expressing GFP-MCOLN3 contained more than 20 autophagosomes after the same recovery period (Figure 8E). Therefore, these results suggest that MCOLN3 overexpression inhibits autophagic degradation. Although we cannot discard that MCOLN3 also enhances autophagosome formation, we did not observed increased levels of beclin-1 in MCOLN3-expressing cells (data not shown).

Altogether, our data reveal that MCOLN3 localizes to the endosomal pathway and is required for efficient sorting of cargo proteins and autophagosomes to lysosomes for degradation.

Overexpression of MCOLN3 alters endosomal pH

To gain additional insight on the function of MCOLN3 at the endosomal pathway we addressed whether MCOLN3 overexpression might alter endosomal pH. The reason for this is that MCOLN3 is a Ca2+ channel and release of Ca2+ has been linked to endosomal acidification (51) (see discussion).

The kinetics of endosomal acidification was measured in control and MCOLN3-expressing cells by fluorescence ratio imaging (52). Cells were simultaneously loaded with fluorescein- and Alexa555-conjugated dextrans. Because fluorescein fluorescence decreases at acidic pH, while Alexa555 fluorescence is pH independent, the ratio of green (fluorescein) to red (Alexa555) fluorescence is indicative of the pH in endocytic vesicles. As shown in Figure 9A endocytic vesicles appear mostly red after 1 h dextran internalization in noninfected cells or cells infected with a control adenovirus, suggesting that at this time point the dextrans have reached an acidic compartment and much of the green fluorescence has been lost. In contrast, most of the green signal is still present in MCOLN3-expressing cells indicating that overexpression of MCOLN3 inhibits proper endosomal acidification.

In a control experiment we determined that MCOLN3 overexpression does not affect trafficking of dextran along the endosomal pathway, as the degree of colocalization of dextran with early endosomal (EEA1) and late endosomal/lysosomal (Lamp-1) markers at different time points was the same in control and MCOLN3-expressing cells (Figure S3).

To convert data to absolute values of pH we measured the fluorescein/Alexa555 ratios and fit them to a curve constructed by calculating ratios in permeabilized cells equilibrated with calibration solutions (Figure 9B). Quantification of many different random fields of cells confirmed that endosomal pH is clearly higher in cells overexpressing MCOLN3. Thus, after 25 min dextran internalization, average endosomal pH was close to 5.5 in noninfected cells (5.38) or in cells infected with a control adenovirus (5.30), whereas the average pH was over 6 (6.20) in MCOLN3-expressing cells (Figure 9C). Therefore, our data suggest that MCOLN3 function is required for efficient acidification of endosomal vesicles. In addition, endosomal acidification is known to be crucial for endosomal maturation and vesicle fusion thus explaining the defective sorting of proteins along the endosomal pathway caused by MCOLN3 overexpression.

Discussion

In this paper we have described the intracellular distribution of MCOLN3, a recently identified Ca2+ channel that belongs to the mucolipin family. We found that MCOLN3 localizes to the plasma membrane and intracellular vesicles in ARPE19 cells. The intracellular vesicles correspond primarily to early and late endosomes as revealed by their colocalization with specific markers. The distribution of MCOLN3 in early endosomes is consistent with the previously described regulation of MCOLN3 channel activity by pH. Thus, MCOLN3 is predicted to be fully active at the characteristic pH of early endosomes (pH ≅6.3) while it would become inactive at the lower pH found in lysosomes (pH ≅4–5.5) (53). In contrast, MCOLN1, another member of the mucolipin family, is activated by very low pH and consequently localizes to late endosomes–lysosomes.

We have also found that overexpressed MCOLN3 localizes to enlarged structures that seem to be early endosomes based on the presence of Hrs. Unfortunately, confocal microscopy could not provide sufficient resolution to discern whether these enlarged structures correspond to swollen endosomes or to groups of normal-sized endosomes clustered together. Furthermore, MCOLN3 overexpression impaired delivery of EGF and EGFR from the plasma membrane to lysosomes, causing retention of EGF in enlarged endosomes and

delayed degradation of both EGF and EGFR. Degradation of cargo coming from the autophagic pathway was also impaired in MCOLN3-expressing cells. MCOLN3 did not affect fusion of autophagosomes with the endosomal pathway but induced accumulation of amphisomes indicating that maturation of amphisomes into autolysosomes was defective. Interestingly, the defects caused by MCOLN3 overexpression (e.g. enlarged endosomes, impaired EGFR degradation and autophagosome maturation) are similar to the ones reported upon overexpression of several proteins involved in the biogenesis of endosomes, such as endosomal sorting complexes required for transport (ESCTRs) (41,54,55) or Hrs (56,57). In addition, depletion of endogenous MCOLN3 by transfection with specific siRNAs accelerated the kinetic of EGFR degradation. Therefore, our results indicate that MCOLN3 may be a novel component of the machinery implicated in the biogenesis and regulation of the endosomal function.

The available evidence indicates that, in addition to Rab and SNARE proteins, release of luminal Ca^{2+} from organelles plays a crucial role in the regulation of many intracellular fusion events. For example, release of luminal Ca^{2+} is required for the homotypic fusion of endosomes (58,59) and the heterotypic fusion of late endosomes with lysosomes (60); however, the channel responsible for releasing Ca^{2+} from these compartments remains to be identified. Interestingly, release of Ca^{2+} seems to be linked to endosomal acidification. Endocytic vesicles contain high levels of Ca^{2+} when they pinch off from the plasma membrane due to the elevated concentrations of this ion in the extracellular medium. Within 20 min, the concentration of Ca^{2+} in the lumen of the early endosomes is dramatically reduced and Ca^{2+} release shows the same time course as endosomal acidification. Furthermore, low extracellular Ca^{2+} concentrations inhibit endosomal acidification without affecting endocytosis, suggesting that Ca^{2+} exit from endosomes is necessary for acidification (51). It has been suggested that the H^+ uptake mediated by the vacuolar H^+ pump may be balanced by Ca^{2+} efflux via endosomal calcium channels. Alternatively, Ca^{2+} release may be necessary to keep K^+ and Cl^- channels open so that charge compensation can occur. MCOLN3 is an excellent candidate to regulate Ca^{2+} efflux from early and late endosomes, as it primarily localizes to these compartments and its activity is regulated by pH. We suggest that MCOLN3 mediates fast Ca^{2+} release from early endosomes, allowing the progressive acidification of this compartment. At lysosomes, when the pH becomes very acidic, the channel activity of MCOLN3 would be inhibited, blocking Ca^{2+} exit (Figure 10). In agreement with this model we found that endosomal pH was considerable higher in cells overexpressing MCOLN3 (Figure 9). The fact that acidification, vesicle fusion and endosome maturation are closely related may explain why overexpression of MCOLN3 causes obvious defects in the trafficking of proteins along the endosomal pathway.

The last few years have seen considerable advances in our understanding of the mucolipin family. Our study provides new evidence indicating that mucolipins distribute to specific locations along the endosomal pathway (MCOLN1-late endosomes/lysosomes; MCOLN2-Arf6 pathway and lysosomes; MCOLN3-early/late endosomes) and play an important regulatory role in the sorting of lipids and proteins. Moreover, we suggest that, in addition to the cytosolic sorting machinery and the lipid compositions of the membranes, the ionic composition of the lumen of cellular organelles also plays a crucial function in the regulation of intracellular trafficking and organelle biogenesis and propose that mucolipins are key components in the regulation of these events.

Materials and Methods

The following mouse monoclonal antibodies were used: clone 14 to EEA1 and clone 23 to Clathrin Heavy Chain (BD Transduction Laboratories), clone H5C6 to CD63 (BD

Pharmingen), clone 6C4 to LBPA (Echlon Biosciences Inc.), clone H4A3 to Lamp-1 (Developmental Studies Hybridoma Bank) and clone FK2 to multi-ubiquitin (MBL International Co.). The following polyclonal antibodies were also used: anti-Hrs (Novus Biologicals), anti-LC3 (Sigma-Aldrich), anti-EGF Receptor (Cell Signaling Technology) and anti-sorting nexin 2 (SNX2) (61). Alexa Fluor 568-conjugated goat anti-rabbit IgG, Alexa Fluor 568-conjugated goat anti-mouse IgG, Alexa Fluor 647-conjugated goat anti-mouse IgG and Alexa Fluor 555-labeled EGF were purchased from Invitrogen. HRP-conjugated anti-mouse or anti-rabbit IgG were acquired from GE Healthcare Bio-Sciences Corp. FuGENE-6 transfection reagent and protease inhibitor cocktail tablets were obtained from Roche Applied Science. Dextran conjugated to fluorescein (pH sensitive) and dextran conjugated to Alexa Fluor 555 (10 000 MW) were from Invitrogen.

Recombinant DNA constructs and adenovirus preparation

The full-length cDNA of human Mucolipin-3 (MCOLN3; GenBankTM/EMBL/ DDBJ accession number NM_018298) was obtained by PCR amplification from a human kidney cDNA library (Clontech Laboratories, Inc.), followed by in-frame cloning into HindIII-EcoRI sites of pmGFP-C1 and pmCherry-C1 vectors, or HindIII-BamHI sites of pCDNA3.1/Hygro(+) vector. Constructs were confirmed by DNA sequencing. GFP-Hrs construct was a kind gift of Silvie Urbe (University of Liverpool, Liverpool, United Kingdom). Control adenovirus and adenovirus expressing GFP, GFP-MCOLN3 or untagged-MCOLN3 were prepared, amplified, and purified by Welgen, Inc.

Cell culture, transfection, siRNA knockdown and adenoviral infection

ARPE19 cells (American Type Culture Collection) were grown at 37^C in a 1:1 mixture of DMEM and Ham's F12 media supplemented with 10% fetal bovine serum (Invitrogen Co.), 2 mm GlutamaxTM, 100 U/mL penicillin, and 100 μg/mL streptomycin in a humidified 5% CO2 atmosphere. Cells were transiently transfected using FuGENE-6 reagent (Roche Applied Science) following manufacturer's recommendations. Transfected cells were analyzed 24–36 h post-transfection. For siRNA knockdown, cells were transfected with either ON-TARGETplus smart pool siRNA duplexes against MCOLN3 or ON-TARGETplus nontargeting pool siRNA duplexes using DharmaFECT transfection reagent (Dharmacon-ThermoScientific). Treated cells were analyzed 72–80 h after transfection. For infection experiments, cells were infected with adenoviruses according to the manufacturer's recommendations. Analyses were performed 36–40 h post-infection.

Immunofluorescence microscopy and internalization assays

For immunofluoresence, cells grown on coverslips were washed with PBS and fixed with 4% paraformaldehyde for 15 min at room temperature or with methanol/acetone (1:1, v/v) for 10 min at −20^C. Cells then were incubated with the indicated primary antibodies in PBS containing 10% Fetal Bovine Serum and 0.1% (wt/v) saponin for 1 h at room temperature, followed by incubation with the corresponding secondary antibodies conjugated to Alexa Fluor568 or Alexa Fluor647. After staining, the coverslips were mounted onto glass slides with Fluoromount-G (SouthernBiotech). For Alexa555-EGF internalization, cells were incubated with Alexa555-EGF (500 ng/mL) in medium containing 0.1% (wt/v) bovine serum albumin for 10 min at 37^C. Cells were then washed with PBS and chased with medium containing BSA for the indicated times at 37^C. Finally, cells were washed two times with PBS and fixed with methanol/acetone as indicated above. Samples were examined and images were acquired on a Zeiss LSM 510 confocal microscope (Carl Zeiss Inc).

For colocalization analysis, the percentage of colocalized vesicles was calculated as the number of GFP-MCOLN3-positive vesicles that colocalized with the indicated organelle

markers divided by the total number of GFP-MCOLN3-positive vesicles in a given cell and multiplied by 100. The same calculation was applied for colocalizations with LC3-positive vesicles.

For starvation and recovery experiments, cells were treated as described previously (19).

Electrophoresis and Immunoblotting

Cells were washed with ice-cold PBS, resuspended in lysis buffer (25 mm Hepes-KOH, pH 7.4, 250 mm NaCl, 1% Triton X-100 (wt/v) supplemented with protease inhibitors cocktail) and lysed by passing the samples 10 times through a 25 gauge needle. Cell lysates were centrifuged at 16 000 × g for 15 min at 4^C, and the soluble fractions were collected. Samples were analyzed by SDS-PAGE (4–20% gradient gels) under reducing conditions and transferred to nitrocellulose. Membranes were immunoblotted using the indicated antibodies. Horseradish peroxidase-chemiluminiscence was developed by using Western Lightning Chemiluminescence Reagent Plus (PerkinElmer Life Sciences).

Degradation of EGFR

Twenty four hours after infection with adenovirus expressing GFP or GFP-MCOLN3, ARPE19 cells were serum-starved for an additional 4 h and then stimulated with EGF (200 ng/mL) in presence of 100 μg/mL cycloheximide for the indicated times at 37^C. Cells were washed with ice-cold PBS, harvested and lysed in Laemmli buffer. Cell extracts were subjected to SDS-PAGE and immunoblotting as described above. The amount of EGFR was quantified by using the public domain software ImageJ version 1.42 (NIMH, NIH), normalized with the clathrin content in the same sample and presented as the fraction of remaining EGFR relative to unstimulated control cells.

EGF internalization

To study the rate of 125I-EGF internalization, ARPE19 cells were cultured in 6-well plates and mock-infected or infected with adenovirus expressing GFP-MCOLN3 for 40 h. Cells were serum-starved for 4 h in internalization medium (IM; 1:1 mixture of DMEM and Ham's F12 media and 20 mm Hepes containing 0.1% BSA), placed on ice, briefly washed one time with ice-cold IM, and incubated for 1 h on a rocker at 4^C in 0.6 mL IM containing 125I-EGF at 300 nCi/mL (1.5 ng/mL). The monolayers were then washed three times with ice-cold IM. To determinate the amount of surface-bound 125I-EGF for the zero time point, one plate of each condition was incubated for 5 min with 0.8 mL of acid wash (0.2 m acetic acid, pH 2.8, containing 0.5 m NaCl) on ice followed by a second short wash with the same acid solution. The remaining plates were incubated with 1 mL of prewarmed I m at 37^C for various times. To stop the internalization process, cells were placed on ice, the incubation medium was collected, and the cell surface-bound 125I-EGF was collected by acid wash as described above. Finally, cells were lysed with 0.8 mL of 1 m NaOH. Radioactivity in the medium, acid wash and NaOH extract was quantified using a gamma counter (PerkinElmer). Non-specific binding was measured for each time point in the presence of 250-fold molar excess of unlabeled EGF and was not more that 1% of the total counts.

RNA isolation

RNA was isolated from cells by using PureLink Total RNA Purification System (Invitrogen Co.) following manufacturer recommendations. RNA yield was quantified by measuring the optical density at 260 and 280 nm using an Eppendorf BioPhotometer.

Quantitative reverse transcription-polymerase chain reaction

RNA (2–4 μg) was reverse transcribed in a 20 μL reaction using oligo(dT)20 and SuperScript III First-Strand Synthesis System (Invitrogen Co.) following manufacturer recommendations. PCR was performed using 5 μL SYBR GreenER qPCR SuperMix (Invitrogen Co.), 2 μL cDNA, 1 μL gene specific primer mix (QuantiTect primer Assays, QIAGEN, Valencia, CA) and 2 μL water for a total reaction volume of 10 μL. Quantification of gene expression was performed using 7900HT Fast Real-Time PCR System (Applied Biosystems). The thermal profile of the reaction was: 50^C for 2 min, 95^C for 10 min and 40 cycles of 95^C for 15 seconds followed by 60^C for 1 min. All samples were run in triplicates. Amplification of the sequence of interest was compared with a reference probe (β-2-microglobulin) and normalized against a standard curve of cell line mRNA. The 7900HT Fast Real-Time PCR System Software was used for data analyses (Applied Biosystems).

Measurement of endosomal pH

ARPE19 cells were grown at 37^C and 5% CO2 in Nunc Lab-Tek chambered cover glasses (Thermo Fisher Scientific Inc.) with DMEM/F12 medium. Cells were incubated for 15 min at 37^C with both 500 μm dextran conjugated to fluorescein (pH sensitive) and 20 μm dextran conjugated to Alexa Fluor 555 (10 000 MW anionic, Invitrogen) in complete growth media. After dextran internalization cells were washed three to five times with complete media and incubate with a physiological buffer (140 mm NaCl, 4.7 mm KCl, 2 mm CaCl2, 1.1 mm MgCl2, 50 mm Hepes, 10 mm glucose, pH 7.4) to be processed for confocal microscopy directly after the rinsing or 1 h after the beginning of the dextran internalization. Confocal microscopy was performed using the 63 × 1.4 NA objective of the Zeiss LSM 510 confocal system equipped with a imaging chamber thermostated at 37^C and maintained at 5% CO2 (Carl Zeiss Inc.). After confocal acquisition, ImageJ version 1.42 software (NIMH, NIH, Bethesda MD) was used to measure the Green/Red fluorescence ratio of the endosomal compartment. Correlation between fluorescence ratio and pH was done by a calibration procedure in a high K+ buffer (44.7 mm NaCl, 100 mm KCl, 2 mm CaCl2, 1.1 mm MgCl2, 50 mm Hepes, 10 mm glucose) supplemented with 5 μm Nigericin (Sigma Aldrich) and a pH set up between 4 and 8.

Supplementary Material

Refer to Web version on PubMed Central for supplementary material.

Acknowledgments

We appreciate the editorial advice of the NIH Fellows Editorial Board. This project was supported by the Intramural Research Program of the NIH, National Heart, Lung, and Blood Institute (NHLBI).

References

1. Amir N, Zlotogora J, Bach G. Mucolipidosis type IV: clinical spectrum and natural history. Pediatrics. 1987; 79:953–959. [PubMed: 2438637]
2. Bach G. Mucolipidosis type IV. Mol Genet Metab. 2001; 73:197–203. [PubMed: 11461186]
3. Altarescu G, Sun M, Moore DF, Smith JA, Wiggs EA, Solomon BI, Patronas NJ, Frei KP, Gupta S, Kaneski CR, Quarrell OW, Slaugenhaupt SA, Goldin E, Schiffmann R. The neurogenetics of mucolipidosis type IV. Neurology. 2002; 59:306–313. [PubMed: 12182165]
4. Vergarajauregui S, Puertollano R. Two di-leucine motifs regulate trafficking of mucolipin-1 to lysosomes. Traffic. 2006; 7:337–353. [PubMed: 16497227]

5. Venkatachalam K, Hofmann T, Montell C. Lysosomal localization of TRPML3 depends on TRPML2 and the mucolipidosis-associated protein TRPML1. J Biol Chem. 2006; 281:17517–17527. [PubMed: 16606612]
6. Pryor PR, Reimann F, Gribble FM, Luzio JP. Mucolipin-1 is a lysosomal membrane protein required for intracellular lactosylceramide. Traffic. 2006; 7:1388–1398. [PubMed: 16978393]
7. Miedel MT, Weixel KM, Bruns JR, Traub LM, Weisz OA. Posttranslational cleavage and adaptor protein complex-dependent trafficking of mucolipin-1. J Biol Chem. 2006; 281:12751–12759. [PubMed: 16517607]
8. Thompson EG, Schaheen L, Dang H, Fares H. Lysosomal trafficking functions of mucolipin-1 in murine macrophages. BMC Cell Biol. 2007; 8:54. [PubMed: 18154673]
9. LaPlante JM, Falardeau J, Sun M, Kanazirska M, Brown EM, Slaugenhaupt SA, Vassilev PM. Identification and characterization of the single channel function of human mucolipin-1 implicated in mucolipidosis type IV, a disorder affecting the lysosomal pathway. FEBS Lett. 2002; 532:183–187. [PubMed: 12459486]
10. Cantiello HF, Montalbetti N, Goldmann WH, Raychowdhury MK, González-Perrett S, Timpanaro GA, Chasan B. Cation channel activity of mucolipin-1: the effect of calcium. Pflugers Arch. 2005; 451:304–312. [PubMed: 16133264]
11. Kiselyov K, Chen J, Rbaibi Y, Oberdick D, Tjon-Kon-Sang S, Shcheynikov N, Muallem S, Soyombo A. TRP-ML1 is a lysosomal monovalent cation channel that undergoes proteolytic cleavage. J Biol Chem. 2005; 280:43218–43223. [PubMed: 16257972]
12. Dong XP, Cheng X, Mills E, Delling M, Wang F, Kurz T, Xu H. The type IV mucolipidosis-associated protein TRPML1 is an endolysosomal iron release channel. Nature. 2008; 455:992–996. [PubMed: 18794901]
13. Vergarajauregui S, Oberdick R, Kiselyov K, Puertollano R. Mucolipin 1 channel activity is regulated by protein kinase A-mediated phosphorylation. Biochem J. 2008; 410:417–425. [PubMed: 17988215]
14. Raychowdhury MK, González-Perrett S, Montalbetti N, Timpanaro GA, Chasan B, Goldmann WH, Stahl S, Cooney A, Goldin E, Cantiello HF. Molecular pathophysiology of mucolipidosis type IV: pH dysregulation of the mucolipin-1 cation channel. Hum Mol Genet. 2004; 13:617–627. [PubMed: 14749347]
15. Soyombo AA, Tjon-Kon-Sang S, Rbaibi Y, Bashllari E, Bisceglia J, Muallem S, Kiselyov K. TRP-ML1 regulates lysosomal pH and acidic lysosomal lipid hydrolytic activity. J Biol Chem. 2006; 281:7294–7301. [PubMed: 16361256]
16. Treusch S, Knuth S, Slaugenhaupt SA, Goldin E, Grant BD, Fares H. Caenorhabditis elegans functional orthologue of human protein h-mucolipin-1 is required for lysosome biogenesis. Proc Natl Acad Sci U S A. 2004; 101:4483–4488. [PubMed: 15070744]
17. Piper RC, Luzio JP. CUPpling calcium to lysosomal biogenesis. Trends Cell Biol. 2004; 14:471–473. [PubMed: 15350973]
18. Miedel MT, Rbaibi Y, Guerriero CJ, Colletti G, Weixel KM, Weisz OA, Kiselyov K. Membrane traffic and turnover in TRP-ML1-deficient cells: a revised model for mucolipidosis type IV pathogenesis. J Exp Med. 2008; 205:1477–1490. [PubMed: 18504305]
19. Vergarajauregui S, Connelly PS, Daniels MP, Puertollano R. Autophagic dysfunction in mucolipidosis type IV patients. Hum Mol Genet. 2008; 17:2723–2737. [PubMed: 18550655]
20. LaPlante JM, Sun M, Falardeau J, Dai D, Brown EM, Slaugenhaupt SA, Vassilev PM. Lysosomal exocytosis is impaired in mucolipidosis type IV. Mol Genet Metab. 2006; 89:339–348. [PubMed: 16914343]
21. Lindvall JM, Blomberg KE, Väliaho J, Vargas L, Heinonen JE, Berglöf A, Mohamed AJ, Nore BF, Vihinen M, Smith CI. Bruton's tyrosine kinase: cell biology, sequence conservation, mutation spectrum, siRNA modifications, and expression profiling. Immunol Rev. 2005; 203:200–215. [PubMed: 15661031]
22. Song Y, Dayalu R, Matthews SA, Scharenberg AM. TRPML cation channels regulate the specialized lysosomal compartment of vertebrate B-lymphocytes. Eur J Cell Biol. 2006; 85:1253–1264. [PubMed: 17050035]

23. Karacsonyi C, Miguel AS, Puertollano R. Mucolipin-2 localizes to the Arf6-associated pathway and regulates recycling of GPI-APs. Traffic. 2007; 8:1404–1414. [PubMed: 17662026]
24. Cools AR. Neurochemical correlates of the waltzing-shaker syndrome in the varitint-waddler mouse. Psychopharmacologia. 1972; 24:384–396. [PubMed: 5064304]
25. Cable J, Steel KP. Combined cochleo-saccular and neuroepithelial abnormalities in the varitint-waddler-J (VaJ) mouse. Hear Res. 1998; 123:125–136. [PubMed: 9745961]
26. Di Palma F, Belyantseva IA, Kim HJ, Vogt TF, Kachar B, Noben-Trauth K. Mutations in Mcoln3 associated with deafnessand pigmentation defects in varitint-waddler (Va) mice. Proc Natl Acad Sci U S A. 2002; 99:14994–14999. [PubMed: 12403827]
27. Kim HJ, Jackson T, Noben-Trauth K. Genetic analyses of the mouse deafness mutations varitint-waddler (Va) and jerker (Espnje). J Assoc Res Otolaryngol. 2003; 4:83–90. [PubMed: 12209292]
28. Atiba-Davies M, Noben-Trauth K. TRPML3 and hearing loss in the varitint-waddler mouse. Biochim Biophys Acta. 2007; 1772:1028–1031. [PubMed: 17329082]
29. Cuajungco MP, Samie MA. The varitint-waddler mouse phenotypes and the TRPML3 ion channel mutation: cause and consequence. Pflugers Arch. 2008; 457:463–473. [PubMed: 18504603]
30. Kim HJ, Li Q, Tjon-Kon-Sang S, So I, Kiselyov K, Muallem S. Gain-of-function mutation in TRPML3 causes the mouse varitint-waddler phenotype. J Biol Chem. 2007; 282:36138–36142. [PubMed: 17962195]
31. Nagata K, Zheng L, Madathany T, Castiglioni AJ, Bartles JR, García-Añoveros J. The varitint-waddler (Va) deafness mutation in TRPML3 generates constitutive, inward rectifying currents and causes cell degeneration. Proc Natl Acad Sci U S A. 2008; 105:353–358. [PubMed: 18162548]
32. Kim HJ, Li Q, Tjon-Kon-Sang S, So I, Kiselyov K, Soyombo AA, Muallem S. A novel mode of TRPML3 regulation by extracytosolic pH absent in the varitint-waddler phenotype. EMBO J. 2008; 27:1197–1205. [PubMed: 18369318]
33. Grimm C, Cuajungco MP, Van Aken AF, Schnee M, Jörs S, Kros CJ, Ricci AJ, Heller S. A helix-breaking mutation in TRPML3 leads to constitutive activity underlying deafness in the varitint-waddler mouse. Proc Natl Acad Sci U S A. 2007; 104:19583–19588. [PubMed: 18048323]
34. Xu H, Delling M, Li L, Dong X, Clapham DE. Activating mutation in a mucolipin transient receptor potential channel leads to melanocyte loss in varitint-waddler mice. Proc Natl Acad Sci U S A. 2007; 104:18321–18326. [PubMed: 17989217]
35. Dunn KC, Aotaki-Keen AE, Putkey FR, Hjelmeland LM. ARPE-19, a human retinal pigment epithelial cell line with differentiated properties. Exp Eye Res. 1996; 62:155–169. [PubMed: 8698076]
36. Aukunuru JV, Sunkara G, Bandi N, Threson WB, Kompella UB. Expression of multi-drug resistance-associated protein (MRP) in human retinal pigment epithelial cells and its interaction with BAPSG, a novel aldose reductase inhibitor. Pharm Res. 2001; 18:565–572. [PubMed: 11465409]
37. Busik JV, Olson LK, Grant MB, Henry DN. Glucose-induced activation of glucose uptake in cells from the inner and outer blood-retinal barrier. Invest Ophthalmol Vis Sci. 2002; 43:2356–2363. [PubMed: 12091438]
38. Schlessinger J. Ligand-induced, receptor-mediated dimerization and activation of EGF receptor. Cell. 2002; 110:669–672. [PubMed: 12297041]
39. Hackel PO, Zwick E, Prenzel N, Ullrich A. Epidermal growth factor receptors: critical mediators of multiple receptor pathways. Curr Opin Cell Biol. 1999; 11:184–189. [PubMed: 10209149]
40. Pacheco CD, Kunkel R, Lieberman AP. Autophagy in Niemann-Pick C disease is dependent upon Beclin-1 and responsive to lipid trafficking defects. Hum Mol Genet. 2007; 16:1495–1503. [PubMed: 17468177]
41. Filimonenko M, Stuffers S, Raiborg C, Yamamoto A, Malerød L, Fisher EM, Isaacs A, Brech A, Stenmark H, Simonsen A. Functional multivesicular bodies are required for autophagic clearance of protein aggregates associated with neurodegenerative disease. J Cell Biol. 2007; 179:485–500. [PubMed: 17984323]
42. Settembre C, Fraldi A, Jahreiss L, Spampanato C, Venturi C, Medina D, De Pablo R, Tacchetti C, Rubinsztein DC, Ballabio A. A block of autophagy in lysosomal storage disorders. Hum Mol Genet. 2008; 17:119–129. [PubMed: 17913701]

43. Seglen PO, Berg TO, Blankson H, Fengsrud M, Holen I, Strømhaug PE. Structural aspects of autophagy. Adv Exp Med Biol. 1996; 389:103–111. [PubMed: 8860999]
44. Ohsumi Y. Molecular dissection of autophagy: two ubiquitin-like systems. Nat Rev Mol Cell Biol. 2001; 2:211–216. [PubMed: 11265251]
45. Yorimitsu T, Klionsky DJ. Autophagy: molecular machinery for self-eating. Cell Death Differ. 2005; 12:1542–1552. [PubMed: 16247502]
46. Tooze J, Hollinshead M, Ludwig T, Howell K, Hoflack B, Kern H. In exocrine pancreas, the basolateral endocytic pathway converges with the autophagic pathway immediately after the early endosome. J Cell Biol. 1990; 111:329–345. [PubMed: 2166050]
47. Punnonen EL, Autio S, Kaija H, Reunanen H. Autophagic vacuoles fuse with the prelysosomal compartment in cultured rat fibroblasts. Eur J Cell Biol. 1993; 61:54–66. [PubMed: 8223708]
48. Liou W, Geuze HJ, Geelen MJ, Slot JW. The autophagic and endocytic pathways converge at the nascent autophagic vacuoles. J Cell Biol. 1997; 136:61–70. [PubMed: 9008703]
49. Berg TO, Fengsrud M, Stromhaug PE, Berg T, Seglen PO. Isolation and characterization of rat liver amphisomes. Evidence for fusion of autophagosomes with both early and late endosomes. J Biol Chem. 1998; 273:21883–21892. [PubMed: 9705327]
50. Gordon PB, Seglen PO. Prelysosomal convergence of autophagic and endocytic pathways. Biochem Biophys Res Commun. 1988; 151:40–47. [PubMed: 3126737]
51. Gerasimenko JV, Tepikin AV, Petersen OH, Gerasimenko OV. Calcium uptake via endocytosis with rapid release from acidifying endosomes. Curr Biol. 1998; 8:1335–1338. [PubMed: 9843688]
52. Dunn K, Maxfield FR. Ratio imaging instrumentation. Methods Cell Biol. 2003; 72:389–441. [PubMed: 14719342]
53. Paroutis P, Touret N, Grinstein S. The pH of the secretory pathway: measurement, determinants, and regulation. Physiology. 2004; 19:207–215. [PubMed: 15304635]
54. Lu Q, Hope LW, Brasch M, Reinhard C, Cohen SN. TSG101 interaction with HRS mediates endosomal trafficking and receptor down-regulation. Proc Natl Acad Sci U S A. 2003; 100:7626–7631. [PubMed: 12802020]
55. Rusten TE, Vaccari T, Lindmo K, Rodahl LM, Nezis IP, Sem-Jacobsen C, Wendler F, Vincent JP, Brech A, Bilder D, Stenmark H. ESCRTs and Fab1 regulate distinct steps of autophagy. Curr Biol. 2007; 17:1817–1825. [PubMed: 17935992]
56. Bishop N, Horman A, Woodman P. Mammalian class E vps proteins recognize ubiquitin and act in the removal of endosomal protein—ubiquitin conjugates. J Cell Biol. 2002; 157:91–101. [PubMed: 11916981]
57. Tamai K, Tanaka N, Nara A, Yamamoto A, Nakagawa I, Yoshimori T, Ueno Y, Shimosegawa T, Sugamura K. Role of Hrs in maturation of autophagosomes in mammalian cells. Biochem Biophys Res Commun. 2007; 360:721–727. [PubMed: 17624298]
58. Holroyd C, Kistner U, Annaert W, Jahn R. Fusion of endosomes involved in synaptic vesicle recycling. Mol Biol Cell. 1999; 10:3035–3044. [PubMed: 10473644]
59. Yan Q, Sun W, McNew JA, Vida TA, Bean AJ. Ca2+ and N-ethylmaleimide-sensitive factor differentially regulate disassembly of SNARE complexes on early endosomes. J Biol Chem. 2004; 279:18270–18276. [PubMed: 14769786]
60. Pryor PR, Mullock BM, Bright NA, Gray SR, Luzio JP. The role of intraorganellar Ca2+ in late endosome–lysosome heterotypic fusion and in the reformation of lysosomes from hybrid organelles. J Cell Biol. 2000; 149:1053–1062. [PubMed: 10831609]
61. Haft CR, De La Luz Sierra M, Bafford R, Lesniak MA, Barr VA, Taylor SI. Human orthologs of yeast vacuolar protein sorting proteins Vps26, 29, and 35: assembly into multimeric complexes. Mol Biol Cell. 2000; 11:4105–4116. [PubMed: 11102511]

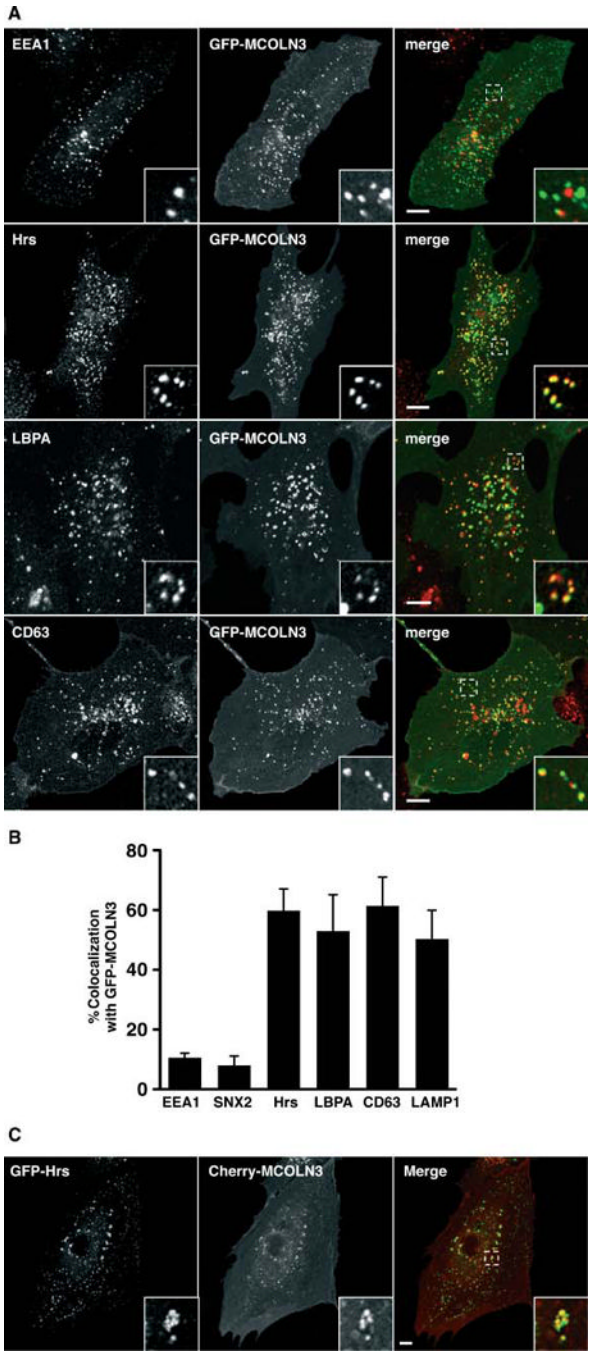

Figure 1.

MCOLN3 distribution in ARPE19 cells. A) ARPE19 cells transiently transfected with GFP-MCOLN3 were fixed, permeabilized, immunostained with the indicated antibodies, and analyzed by confocal fluorescence microscopy. Insets show a fourfold magnification of the indicated region. B) Quantification of the colocalization between vesicles containing GFP-MCOLN3 and various organelle markers. Results are mean ± SD. C) Cells transiently cotransfected with GFP-HRS and Cherry-MCOLN3 were analyzed as indicated in (A). Insets show a fourfold magnification of the indicated region. Scale bar: 10 μm.

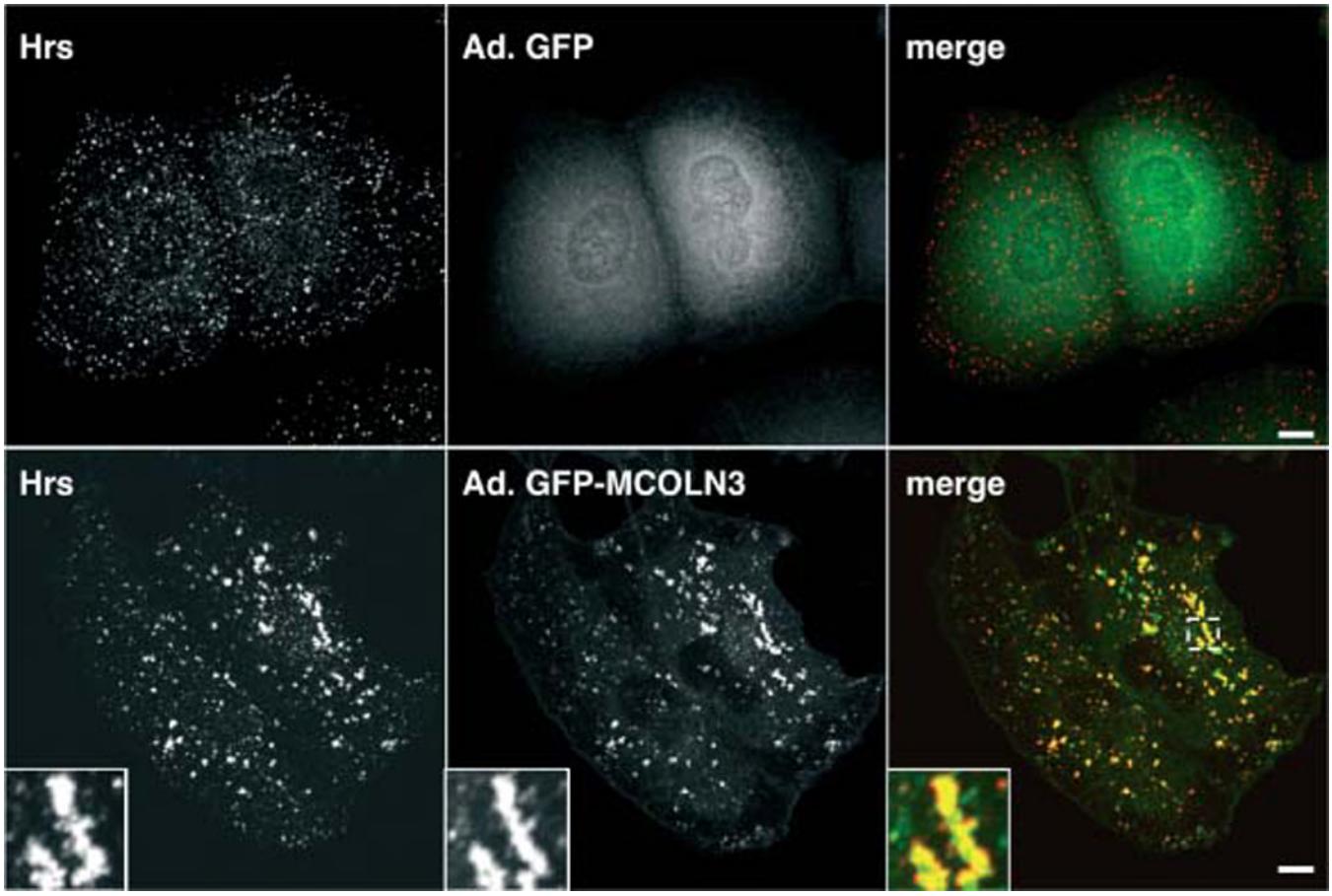

Figure 2.
MCOLN3 overexpression induces accumulation of enlarged endosomes. ARPE19 cells infected with adenovirus expressing either GFP (upper panel) or GFP-MCOLN3 (lower panel) were fixed, permeabilized, and immunostained with antibodies to Hrs. Insets show a fourfold magnification of the indicated region. Scale bar: 10 μm.

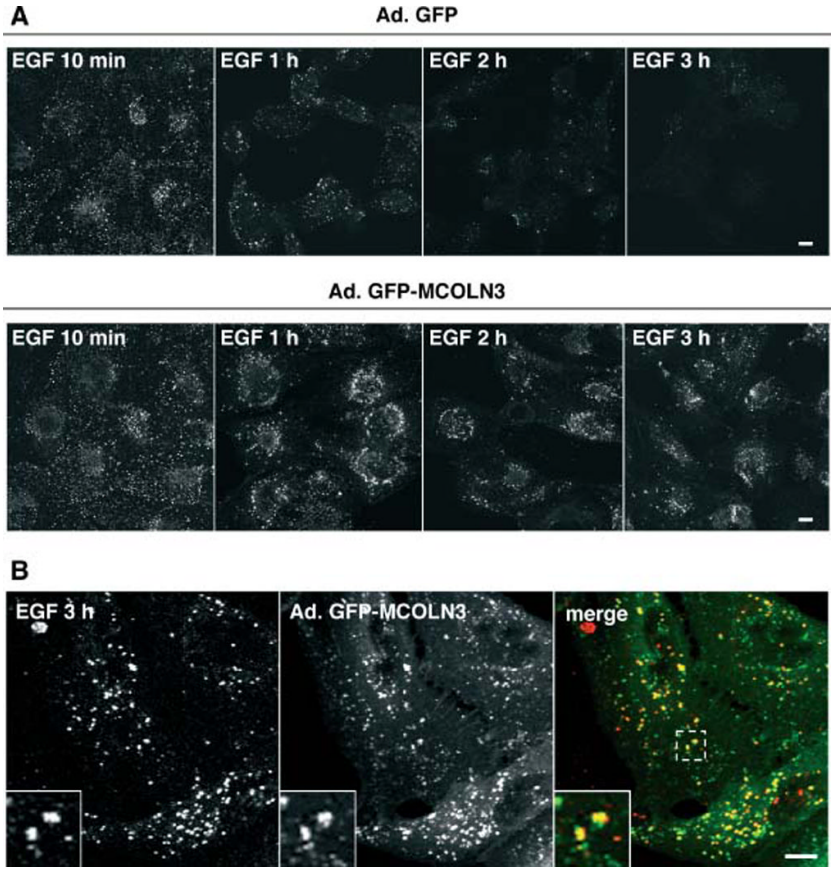

Figure 3.

Overexpression of GFP-MCOLN3 delays degradation of Alexa555-labeled EGF. A) ARPE19 cells were infected with adenovirus expressing either GFP (upper panel) or GFP-MCOLN3 (lower panel). Infected cells were incubated with Alexa555-labeled EGF for 10 min at 37^C. Cells were then washed, incubated with complete medium for the indicated length of time, fixed and analyzed by confocal fluorescent microscopy. Note that in cells expressing GFP-MCOLN3, Alexa555-labeled EGF is still present in intracellular structures after 3 h internalization. In contrast no Alexa555-labeled EGF was detected in GFP expressing cells. B) Cells infected with adenovirus expressing GFP-MCOLN3 were incubated with Alexa555-labeled EGF for 3 h and analyzed as indicated in (A). Note that after 3 h of internalization Alexa555-labeled EGF remained trapped at endosomes that also contain GFP-MCOLN3. Insets represent a threefold magnification of the indicated area. Scale bar: 10 μm.

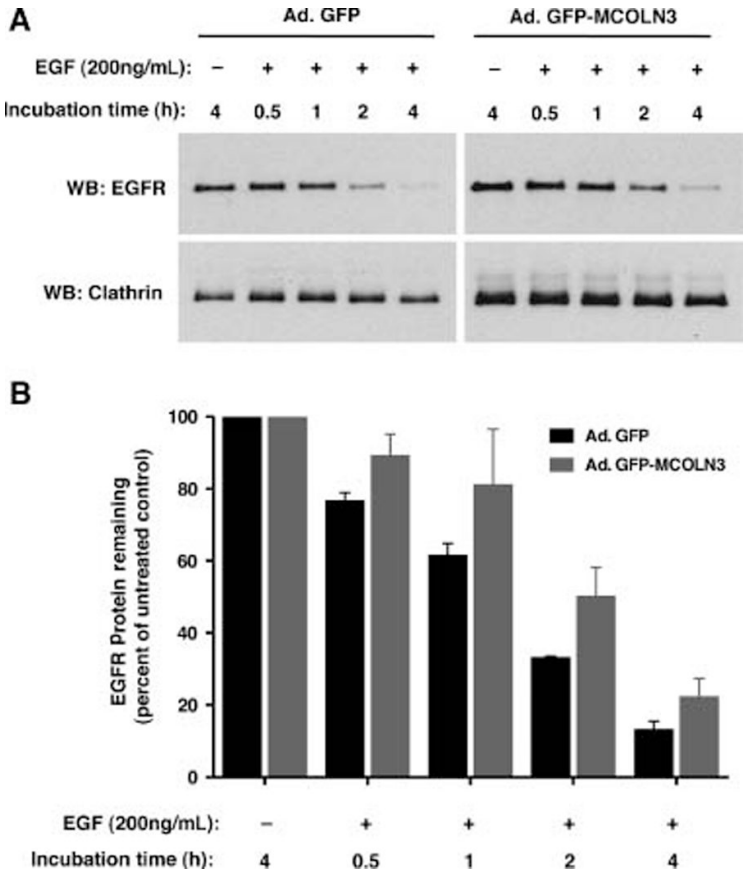

Figure 4.

Overexpression of GFP-MCOLN3 affects normal trafficking of EGFR along the endo/lysosomal pathway. A) ARPE19 cells infected with adenovirus expressing either GFP or GFP-MCOLN3 were starved for 4 h in medium containing 0.1% BSA and incubated with or without 200 ng/mL of EGF for the indicated times. Cells were then processed for Western blot to detect EGFR and clathrin (loading control). B) Quantification of the Western blots in (A). EGFR has been normalized to the clathrin content in the same sample. Bars represent the mean ± SD of three independent experiments.

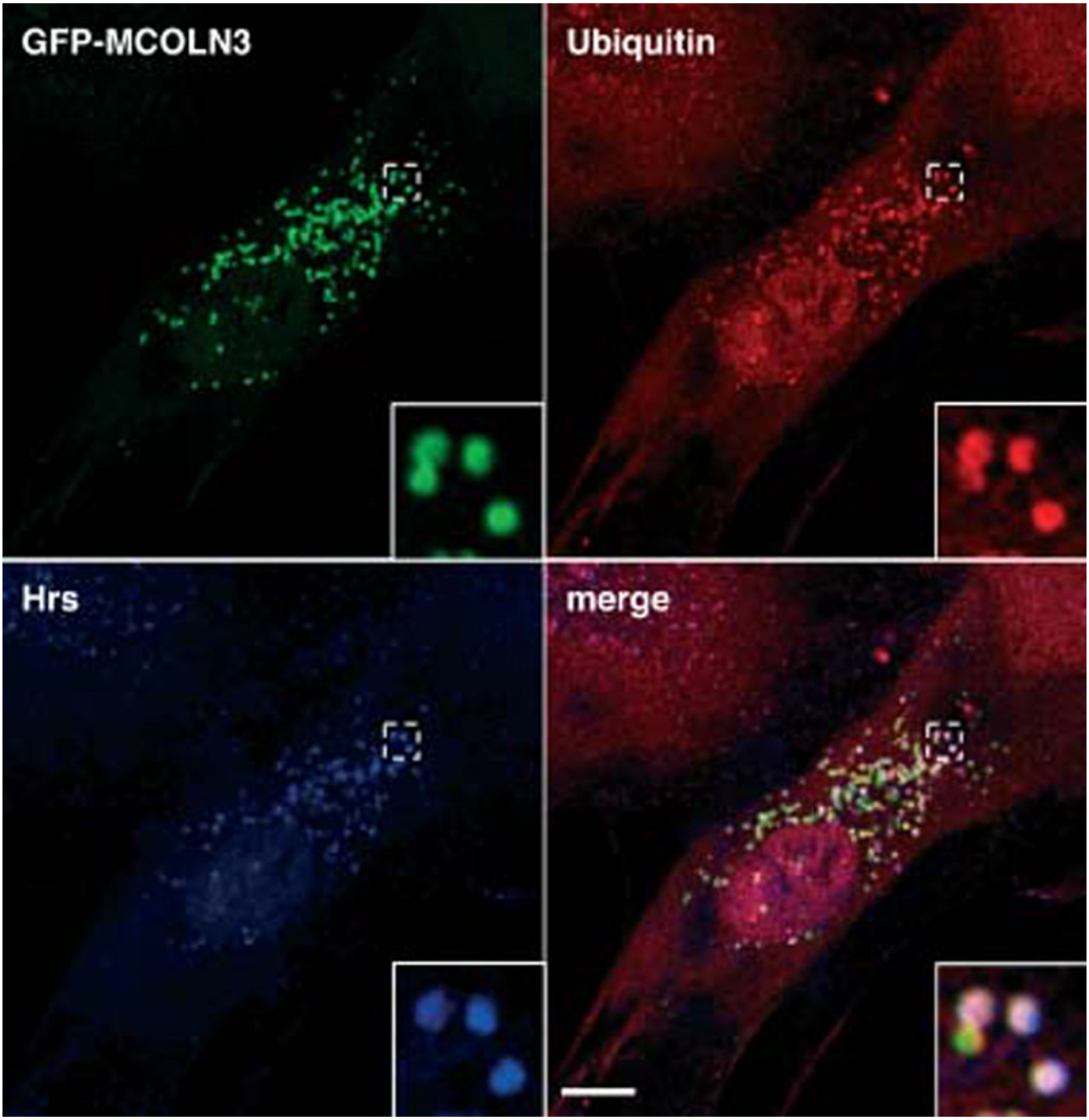

Figure 5.
MCOLN3 overexpression induces accumulation of ubiquitinated proteins in endosomes. ARPE19 cells were transiently transfected with GFP-MCOLN3, fixed, permeabilized, immunostained with the indicated antibodies, and analyzed by confocal fluorescence microscopy. Insets show a fivefold magnification of the indicated region. Scale bar: 10 μm.

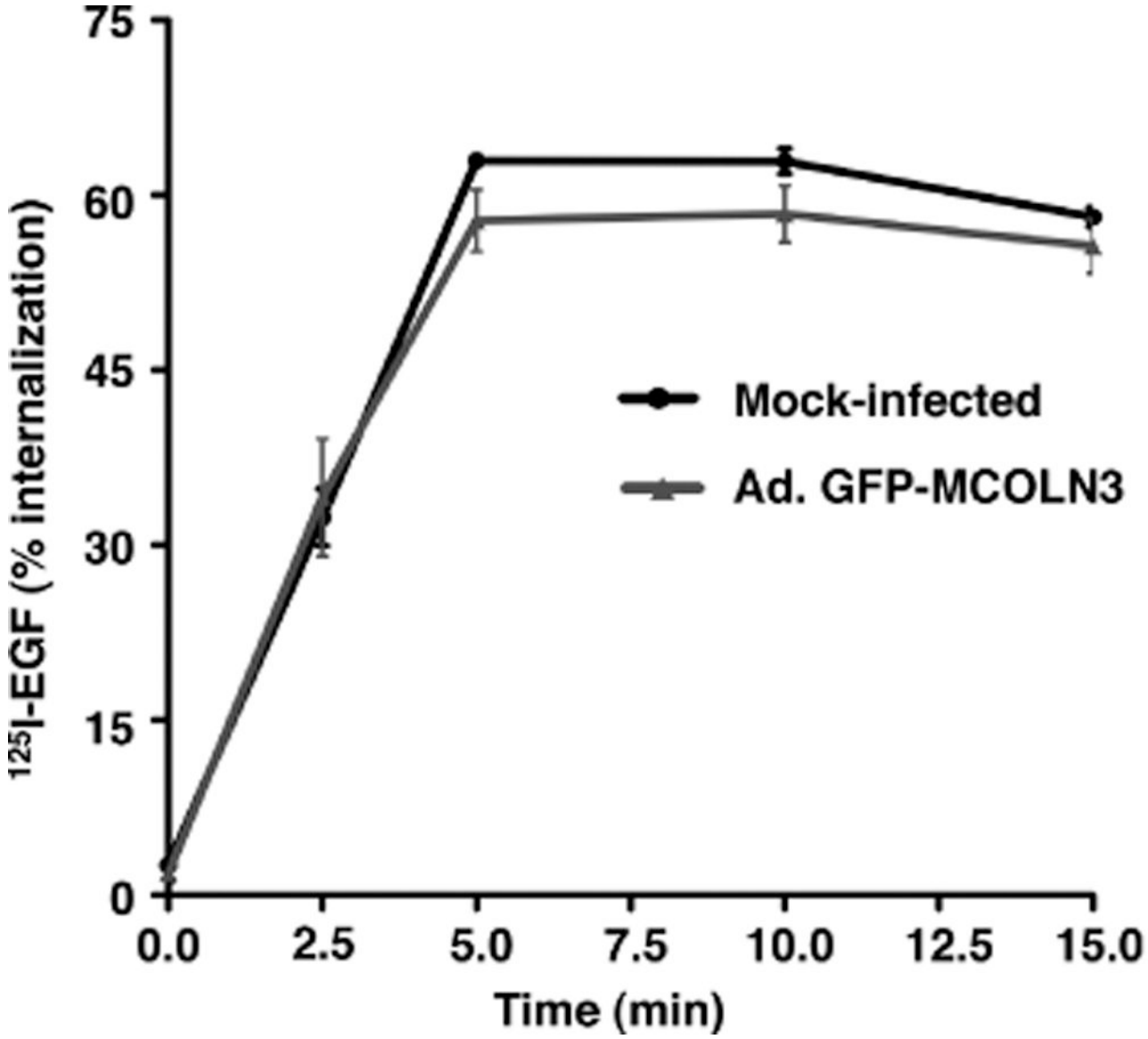

Figure 6.

Overexpression of GFP-MCOLN3 does not affect internalization of EGFR. ARPE19 cells mock-infected (●) or infected with adenovirus expressing GFP-MCOLN3 (▲) were starved for 4 h in medium containing 0.1% BSA. Cells were allowed to bind 125I-EGF at 4^C and then were incubated at 37^C for the indicated times. Medium was collected, ligand remaining on the cell surface was released with an acid wash and the cells were extracted with NaOH. All three fractions were quantified and expressed as a percentage of internalization. Results are mean ± SD of three independent experiments performed in duplicate.

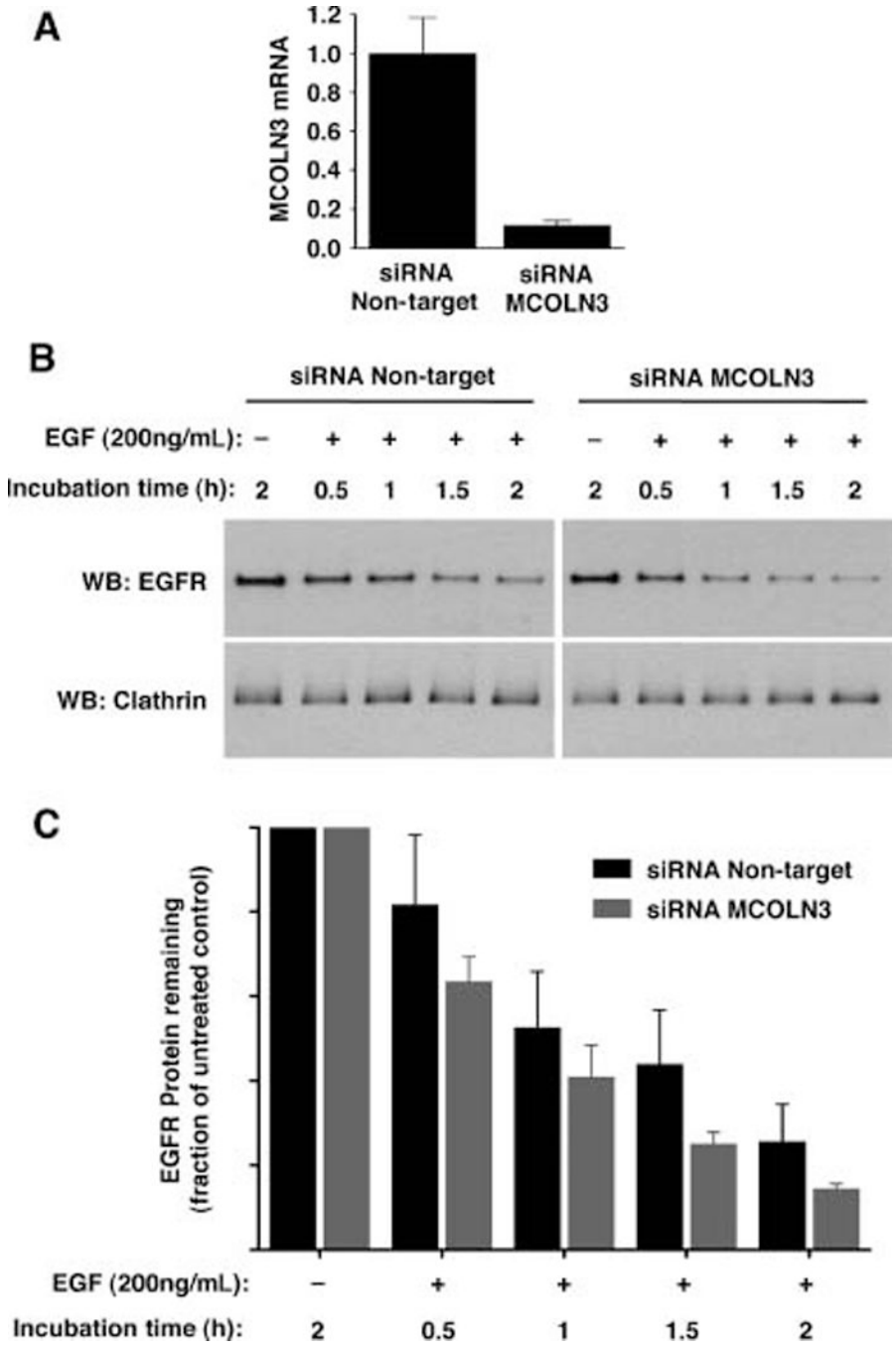

Figure 7.

Depletion of MCOLN3 accelerates degradation of EGFR. A) Q-RT-PCR analysis of MCOLN3 mRNA levels from ARPE19 cells treated with either siRNA nontarget or siRNA to MCOLN3. Results are mean ± SD (n = 3). B) ARPE19 cells treated with siRNA duplexes as indicated in (A) were serum-starved for 4 h in medium containing 0.1% BSA and incubated with or without 200 ng/mL of EGF for the indicated times. Cells were then processed for Western blot to detect EGFR and clathrin (loading control). C) Quantification of the Western blots in (B). EGFR has been normalized to the clathrin content in the same sample. Bars represent the mean ± SD of three independent experiments.

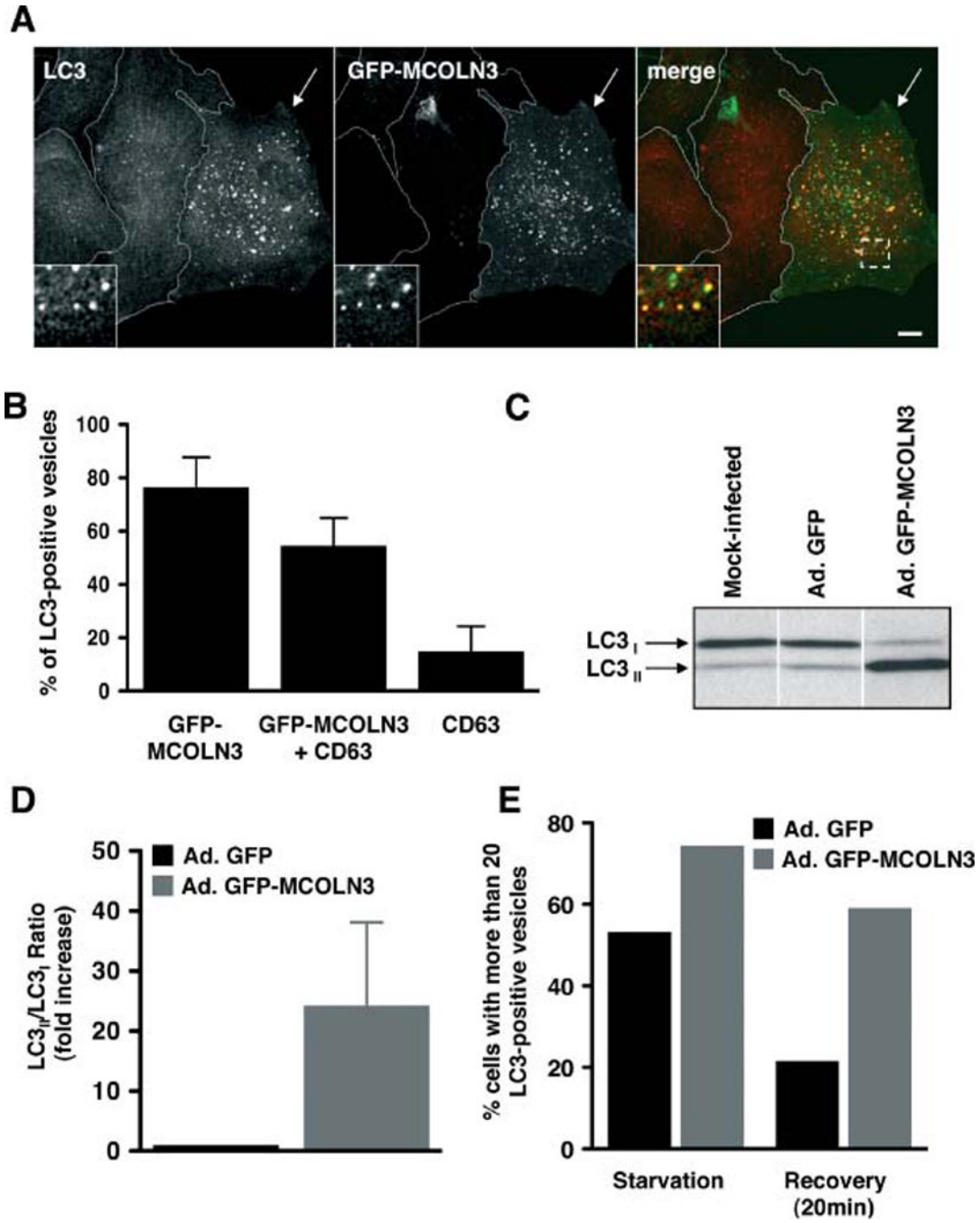

Figure 8.

Overexpression of GFP-MCOLN3 inhibits autophagosome degradation. A) ARPE19 cells transiently transfected with GFP-MCOLN3 were fixed and immunostained to detect LC3. The arrow points to a GFP-MCOLN3 expressing cell. Dotted lines delineate untransfected cells. Insets show a fourfold magnification of the indicated region. Scale bar: 10 μm. B) ARPE19 cells transfected as in (A) were coimmunostained to detect LC3 and CD63. The mean ± SD from 1015 LC3-positive structures is plotted. C) ARPE19 cells mock-infected or infected with adenovirus expressing either GFP or GFP-MCOLN3 were harvested and subjected to Western blotting to detect LC3. The blot shown is representative of four independent experiments. D) Quantification of the Western blot in (C). The ratio of LC3II/

LC3I expressed as a fold-increase of the ratio from cells infected with adenovirus expressing GFP is plotted. Results are the mean ± SD from four independent experiments. (E) ARPE19 cells infected as in (C) were starved in EBSS media for 3 hours and then allowed to recover for 20 min in complete medium. Cells were fixed and LC3-positive structures were analyzed by confocal fluorescence microscopy. The percentage of cells with more than 20 LC3-positive vesicles is plotted.

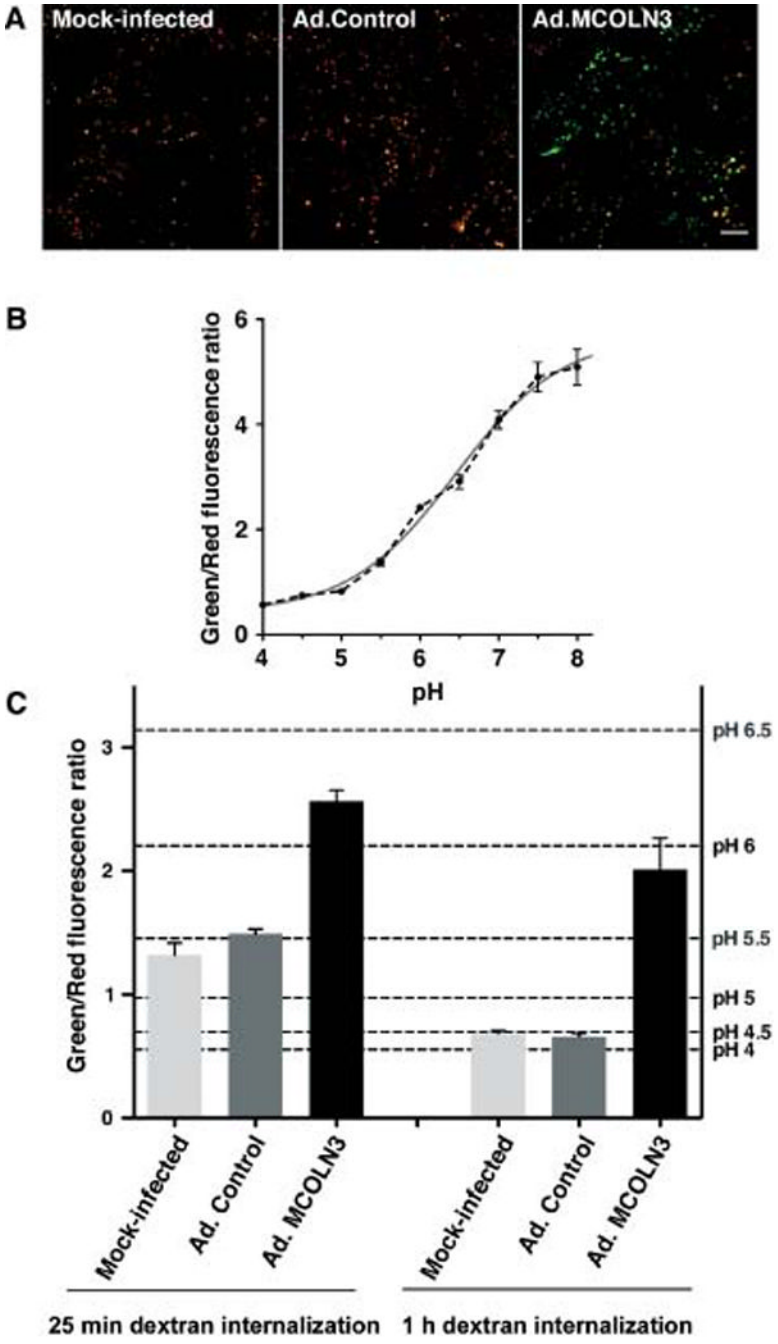

Figure 9.

MCOLN3 overexpression decreases acidification of the endosomal pathway. A) ARPE19 cells were mock-infected, infected with a control adenovirus encoding only the cytomegalovirus (CMV) promoter (Ad. Control), or infected with an adenovirus expressing untagged MCOLN3 (Ad. MCOLN3). For these three conditions cells were incubated 15 min with both fluorescein (green fluorescence, pH sensitive) and Alexa Fluor 555 (red fluorescence, nonsensitive to pH) conjugated dextrans. Live cell images were acquired by confocal microscopy as described in Material and Methods. Confocal images show the overlay of green and red fluorescences after 1-h internalization (15-min incubation with dextrans followed by 45-min chase). Scale bar: 10 μm. B) Correlation between fluorescence

ratio and pH was done on noninfected cells by a calibration procedure with a high potassium buffer in presence of nigericin. Dots represent the mean ± SEM of two to four independent experiments (20–40 random fields of cells) for each pH value. C) Quantification of vesicular fluorescence ratio (left axis) and corresponding pH (right axis, dotted lines) was made after 25 min (15 min incubation with dextrans plus 10 min chase) or 1 h (15 min incubation with dextrans plus 45 min chase) internalization. Bars represent mean ± SEM of three or four independent experiments (29–45 random fields of cells) for each group. Differences in pH between control and MCOLN3-expressing cells were highly statically significant ($p < 0.001$).

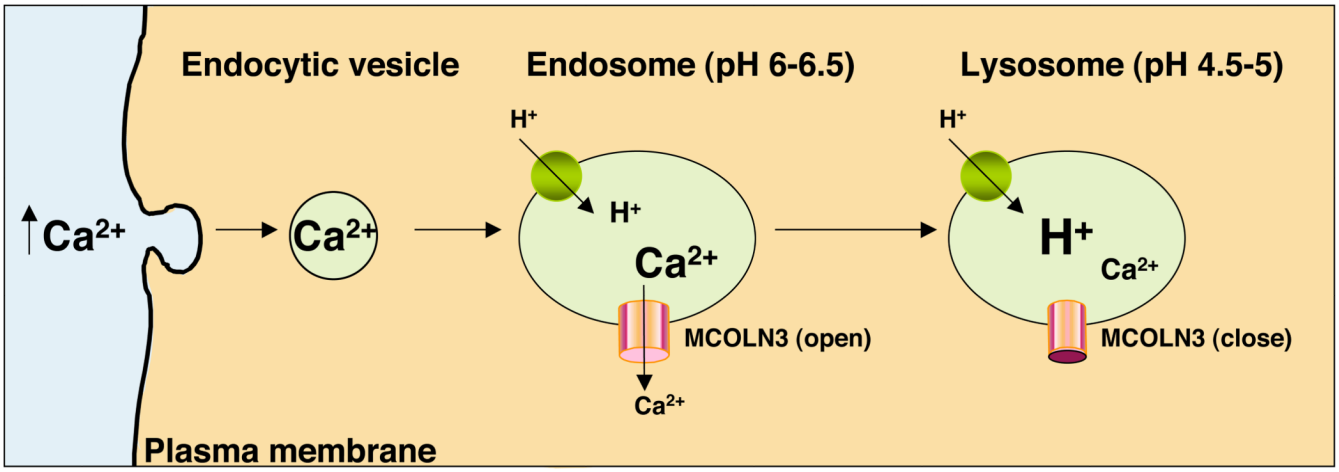

Figure 10.

Proposed model for MCOLN3 function at endosomes. Endocytic vesicles contain high Ca2+ concentrations after being endocytosed from the plasma membrane. Shortly after internalization there is a rapid release of Ca2+ from early endosomes that is necessary to allow acidification of this compartment. We propose that MCOLN3 mediates Ca2+ efflux, as the channel is predicted to be active at the characteristic pH of endosomes (pH 6–6.5). Once late endosomes or lysosomes become highly acidic, the low pH inhibits MCOLN3 channel activity, stopping Ca2+ exit and preventing further acidification. Therefore, MCOLN3 may mediate endosome acidification and maturation. In addition, released Ca2+ might regulate fusion and fission events along the endosomal/lysosomal pathway.